J. Earth Syst. Sci. (2020)129 69
https://doi.org/10.1007/s12040-020-1348-6

© Indian Academy of Sciences

Shell weights of foraminifera trace atmospheric CO_2 from the Miocene to Pleistocene in the central Equatorial Indian Ocean

Tanvi V Mungekar[1], Sushant S Naik[1,*], B Nagender Nath[1] and Dhananjai K Pandey[2]

[1] *CSIR-National Institute of Oceanography, Dona Paula, Goa 403 004, India.*
[2] *National Centre for Polar and Ocean Research, Vasco da Gama, Goa 403 804, India.*
**Corresponding author. e-mail: sushant@nio.org*

MS received 2 August 2019; revised 6 December 2019; accepted 12 December 2019

The Maldives Sea is a region dominated by the South Asian monsoon (SAM) and at present, a CO_2 source to the atmosphere. Ti/Al elemental ratios from Site U1467 and U1468 recovered from the Maldives Sea show a gradual increase from ∼12 Ma and indicate terrigenous inputs to this region associated with increasing wind intensity associated with initiation of the SAM. Shell weights of planktonic foraminifera, *Globigerinoides trilobus* have been used to understand variations in surface water carbonate ion concentration for the last 20 Ma. Shell weights show a good correspondence with global CO_2 records and show heavier shell weights during the colder periods than compared to warmer intervals which reveals that the Maldives Sea behaved similar to other tropical oceanic regions in terms of its surface water carbonate chemistry. A significant decrease in $CaCO_3$ wt.%, decrease in foraminifera shell weights and dissolution of spines along with an increase in organic carbon (OC%) towards 10.5 Ma is linked to the reduced carbonate deposition and increased productivity during monsoon which is a feature in all tropical sediment cores. Lower shell weights and dissolution features on foraminiferal shells were observed during periods of intense Oxygen Minimum Zone (OMZ) suggesting calcite dissolution due to an increase in bottom water CO_2.

Keywords. Maldives Sea; Equatorial Indian Ocean; shell weight; foraminifera; pCO_2; South Asian monsoon.

1. Introduction

The Neogene period was characterized by major changes in sea level and ocean circulation, along with fluctuations and intensification of the South Asian monsoon (SAM) at ∼12.9 Ma, of which the Maldives carbonate edifice bears a tropical marine record (Betzler *et al.* 2016). The Neogene period experienced a warm period, the Miocene Climatic Optimum (MCO) which occurred in late Early Miocene ∼17 Ma and was associated with warming of mid-latitudes by 6°C than present (Flower and Kennett 1994), followed by a transition period, the middle Miocene Climate Transition (MMCT) which marks the period of climate cooling, increased ice sheets and lowering of global sea-level (Miller *et al.* 2005). The initiation of Northern Hemisphere glaciation (NHG) during late Pliocene (∼2.8 Ma) was the last major climate transition in the Cenozoic (Maslin *et al.* 1998).

Published online: 15 February 2020

The phased uplift of Himalayan–Tibetan complex is said to be a major reason for the onset or intensification of the SAM (Zhisheng *et al.* 2001). Long records of the SAM from the Indian Ocean are few (Kroon *et al.* 1991; Gupta *et al.* 2004, 2015; Clift *et al.* 2008; Betzler *et al.* 2016, 2018; Tripathi *et al.* 2017; Bialik *et al.* 2019). Various studies have fixed the timing of monsoon intensification between 30 and 7 Ma (Ramstein *et al.* 1997; Fluteau *et al.* 1999; Gupta *et al.* 2004; Clift *et al.* 2008). Amongst the ongoing discussions on SAM initiation, Betzler *et al.* (2016) provided an age of 12.9 Ma for the onset of an abrupt SAM. Associated with the monsoons is upwelling, especially in coastal regions as seen in the Arabian Sea which makes the Arabian Sea a large CO_2 source to the atmosphere (Goyet *et al.* 1998; Sarma *et al.* 2003). Observations suggest that the Indian Ocean north of 10°S is a net source for atmospheric CO_2, i.e., positive sea–air CO_2 flux (Sarma *et al.* 2013). Though monsoon records as discussed are available, pCO_2 records from the Indian Ocean are rare (Foster *et al.* 2012) and are mainly from regions that have surface seawater CO_2 in equilibrium with the atmosphere. Increase in surface water pCO_2 leads to a decrease in surface water $[CO_3^{2-}]$, one of the important carbonate system parameter, thus decreasing the capacity of foraminifera to calcify and hence the lighter shells (Barker and Elderfield 2002). Shell weights of planktonic foraminifera have the potential to trace atmospheric CO_2 through resultant changes in $[CO_3^{2-}]$ of surface waters (Barker and Elderfield 2002; Naik *et al.* 2010), however, other factors could also influence shell calcification (de Villiers 2004; Beer *et al.* 2010; Naik *et al.* 2013). Oceanic regions dominated by monsoon nurture optimum growth conditions for specific species of planktonic foraminifera during intense monsoon conditions which can be the primary influence on shell calcification and lead to heavier shell weights (Naik *et al.* 2013). There is also a critical gap in understanding the evolution of the carbonate system during the Miocene and Pliocene (Sosdian *et al.* 2018). We therefore attempt to understand the changes in carbonate ion concentration of surface waters by using shell weights of planktonic foraminifera in a region which is presently an atmospheric CO_2 source. We utilize two sites U1467 and U1468 (IODP Expedition 359) covering the last 20 Ma to understand (i) changes in the carbonate ion concentration of surface waters associated with large climatic shifts of the last 20 Ma, and (ii) the effect of SAM on shell calcification in this region.

2. Study area

The Maldives carbonate platform is situated in a regime of strong seasonal climatic and oceanographic variations related to the Asian monsoonal system. During winter monsoon or the northeast monsoon (November–March), the easterly winds deepen the mixed layer, but the inflow of low salinity water mass from Bay of Bengal (Schulte *et al.* 1999) leads to reduced primary productivity. During summer monsoon or southwest monsoon (June–September) the wind fields have westerly configurations and the current pattern is dominated by the eastward flowing Summer Monsoon Current (SMC) whose velocities increase south of Sri Lanka (Tomczak and Godfrey 2003). A thin low-salinity (5–10 m thick) layer overlains the upwelled water due to local precipitation during summer monsoon periods and hence reduces the effect of upwelling at sea surface though the thermocline is shallow. During the inter-monsoon phase (April–June) an anti-cyclonic circulation is developed in the northwestern Indian Ocean due to strong eastward flow of wind across the equatorial region, whereas the transition to winter monsoon (October–November) witnesses the replacement of East Arabia Current (EAC) by the East Indian Winter jet that flows in opposite direction (eastwards along equator) around southern part of India. Thus the primary productivity reaches its maximum during the inter-monsoon months (Schulte *et al.* 1999) due to stronger Indian Ocean Equatorial Westerlies (IEW).

3. Materials and methods

The samples used in the present study were obtained onboard the JOIDES Resolution, during IODP Expedition 359. The sites U1467 and U1468 were drilled in the Inner Sea of Maldives, equatorial Indian Ocean, at a water depth of 487.4 and 521.45 m, respectively (figure 1a and b). Site U1467 is located at 4°51.02′N, 73°17.02′E, and is the eastern-most site located in the Inner Sea. Site U1468 is located at 4°55.98′N, 073°4.28′E, in the Kardiva channel of Inner Sea. These sites lie within the present day Oxygen Minimum Zone (OMZ)

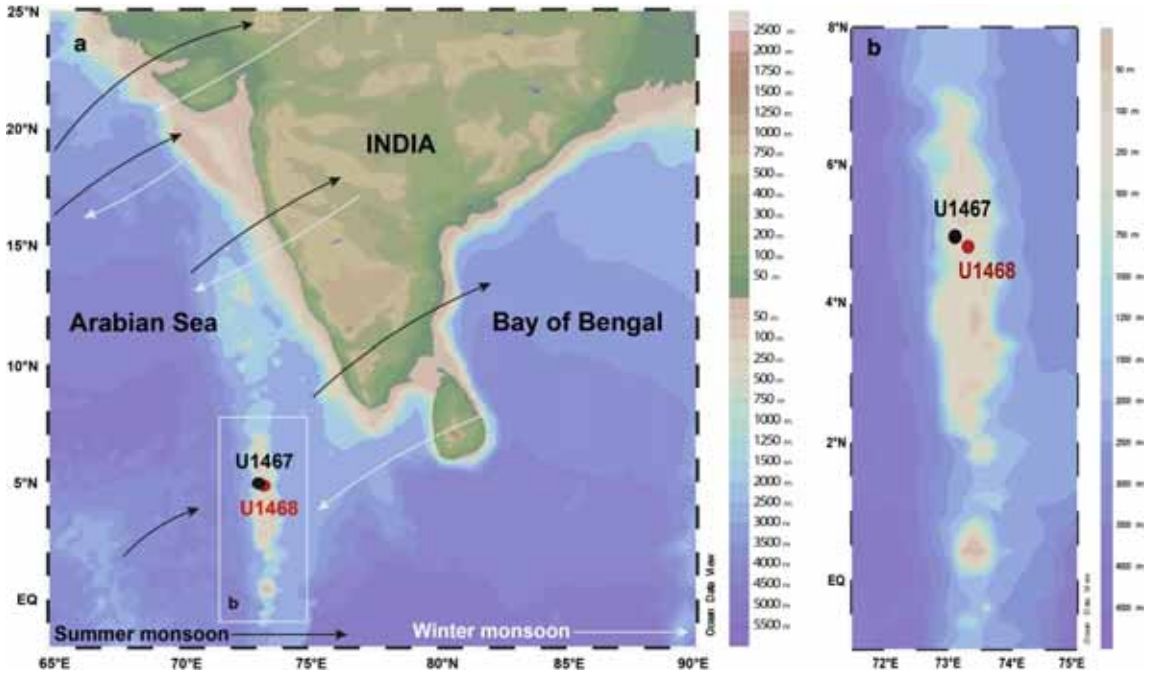

Figure 1. **(a)** Location of Maldives with major wind directions during the summer and winter monsoon indicated by black and white arrows, respectively. **(b)** The black and red dots indicate the location of the sites used in this study.

(Betzler *et al.* 2016). These sites were located at 5°S during late Oligocene (∼31 Ma) and attained the present position (4.5°–5°N) around 20 Ma (van Hinsbergen *et al.* 2015).

The age model was established by using the biostratigraphic events with respect to the first occurrence (FO) and last occurrence (LO) of well-established diagnostic species which are tied to the geomagnetic polarity timescale of Holbourn *et al.* (2005) (Betzler *et al.* 2016, 2017, 2018). Furthermore, calcareous nannofossils and foraminifera were studied from core sections for a refined age determination (Betzler *et al.* 2016). For the calcareous nannoplankton, the standard zonal scheme of Martini (1971) was adopted as a general frame of reference (Betzler *et al.* 2018). Information on the reliability, definition, and timing of events was provided using the compilations of Backman *et al.* (2012) and Raffi *et al.* (2006). Furthermore, a direct correlation of the seismic stratigraphy and the biostratigraphy was achieved. The core to seismic correlation relies on an accurate P wave velocity model for time–depth conversion (Betzler *et al.* 2018). Dating of the drift onset was a high-priority and this key interval was cored at four sites. An age of 12.9 Ma was arrived at with an uncertainty of ca. +/− 0.4 Ma (Betzler *et al.* 2016). In this study, sites U1467 and U1468 were used in conjunction to obtain a total age of 20 Ma.

All analyses were carried out at the CSIR-National Institute of Oceanography, Goa. The sediment samples were disaggregated by soaking in distilled water and were wet sieved with a mesh size of >63 μm. The samples were oven dried at about 60°C and the coarser material was further sieved in size range of 300–355 μm. Planktonic foraminifera, *Globigerinoides trilobus* (∼50 shells) were picked using a stereo-zoom binocular microscope (Meiji Techno EMZ-5) for shell weight analysis. Care was taken to eliminate shells with overgrowths of secondary calcite or any textural changes due to recrystallization or those with infilling of detrital material and coccoliths. The shells were weighed on a microbalance (Sartorius me5) with a precision of ±1 μg. The >125 μm fraction was divided by a microsplitter to obtain around 300 specimens of foraminifera. The ratio between planktonic (P) and benthonic (B) is expressed as plankton percentage of foraminifera fauna: [P/(P+ B) × 100%] (Nigam and Henriques 1992).

For the analyses of titanium and aluminum, about 50 mg of sediment was weighed in a Teflon beaker. 10 ml of acid mixture in the ratio (7:3:1) of HF + HNO_3 + $HClO_4$ was added and heated on a hot plate. Rhodium was used as an internal standard and final solutions were made in an HNO_3 medium. The solution was then diluted to 100 ml by adding ultrapure water (18.2 MΩ). These

solutions were analyzed on a Perkin–Elmer OPTIMA 7300 DV Simultaneous ICP-OES. Marine mud sediment standard (MAG-1) of the United States Geological Survey and stream sediment standard (JSd-1) of Geological Survey of Japan were analyzed along with samples. The precision of measurements as indicated by duplicate samples is ±2% and the accuracy of the analytical results is within ∼5%. Finely ground sediment samples were used for the analysis of total and inorganic carbon. Inorganic carbon (IC) content was determined with a coulometer (UIC, Inc-CM5130 acidification module) and expressed as $CaCO_3$%. Analytical grade calcium carbonate was used as a standard reference material. The precision of measurements were better than ±2%. Total carbon (TC) was measured with a Thermo Flash 2000 CHN-elemental analyzer. The results have a precision within ±3% as obtained for NC soil standard. OC% (organic carbon) was calculated as the difference between TC and IC. Scanning electron micrographs (SEMs) were taken on a 6360 LV, JEOL instrument.

4. Results

Globigerinoides trilobus shell weights show maximum values during the colder periods and range from 15.5 to 27.6 µg for the last 20 Ma. Lowest shell weights, of 15.5 µg were noted during the warm MCO and heaviest shells of 27.6 µg at ∼12.07 Ma (figure 2a). There is also a marked low in shell weights at ∼10.5 Ma. Heavier shells were observed during the Miocene glaciations (Mi2 to 6) and also during the initiation of the NHG. In general, shell weights show an increasing trend in accordance with decreasing atmospheric CO_2 except for the last 1 Ma where shell weights decrease drastically (figure 2a). Planktonic/benthic ratios were also analysed at key intervals within the core and expressed as planktonic% (figure 2a). The planktonic% was noted to be >90% in all the samples analysed, which suggests that the site is from a pelagic realm.

Ti/Al ratios range from 0.01 to 0.1 and in general show a gradual increase beginning from ∼12 Ma (figure 2c). There is a sharp drop in Ti/Al at ∼5 Ma which recovers instantly and the ratios increase further gradually. The organic carbon content (OC%) varied between 0.2 and 6% with episodic higher values throughout the cores and a major increase in OC% towards 10.5 Ma

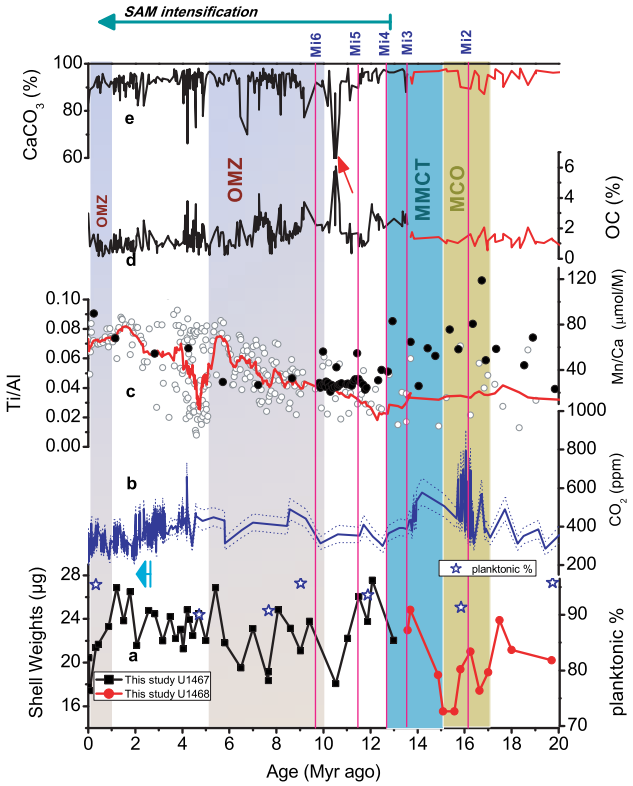

Figure 2. **(a)** Shell weight of planktic foraminifera *Globigerinoides trilobus* (300–355 µm size fraction) from sites U1467 and U1468 combined to cover the last 20 Ma, and planktonic to benthic ratio expressed as percentage of planktonic foraminifera. **(b)** Reconstructed CO_2 record from Sosdian *et al.* (2018) compiled to produce an average curve for the last 20 Ma. The dotted lines show 66% confidence intervals. **(c)** Ti/Al ratios for both the sites, U1467 and U1468 shown as circles. The red line shows running average of the data. Also plotted are the Mn/Ca ratios (Betzler *et al.* 2016) from these sites showing there was a stable OMZ during 10–5 Ma. **(d)** Organic carbon % for the last 20 Ma. **(e)** $CaCO_3$ wt.% for the same period. Red arrow marks the carbonate impoverishment event at ∼10.5 Ma. The warm Miocene Climatic Optimum (MCO) and cold middle Miocene Climate Transition (MMCT) are marked with yellow and blue bands, respectively. The Miocene glacial events Mi2 to Mi6 (Miller *et al.* 1991) are marked by vertical red lines. South Asian Monsoon (SAM) intensification (Betzler *et al.* 2016) is marked by the green arrow on top of the figure. Period of stable OMZ in the Maldives Sea (Betzler *et al.* 2016) and Arabian Sea (Tripathi *et al.* 2017) are marked by colour gradient bands. The initiation of Northern Hemisphere glaciation (NHG) (Maslin *et al.* 1998) is shown by a blue arrow.

(figure 2d). $CaCO_3$% varied between 58 and 98% (figure 2e). $CaCO_3$% at these sites remained high almost throughout the entire period due to continuous carbonate deposition (Betzler *et al.* 2016), except for some events at ∼6.5 to 7 and ∼10 to 10.5 Ma where it dropped to 59% (figure 2e). Both $CaCO_3$% and OC% variations increased after ∼13 Ma when the sea level controlled sedimentation

changed to a current controlled one due to intensification of the SAM (Betzler *et al.* 2016).

5. Discussion

The Maldives region is largely affected by the monsoon system and its associated wind regime. Shamal winds, northwesterly in direction, develop with the low-pressure monsoon system over India and carry dust from nearby western and northwestern deserts up to the equatorial Indian Ocean (Lindhorst *et al.* 2019). The core location is however shielded by atolls from riverine terrestrial input (Betzler *et al.* 2016, 2018; Bunzel *et al.* 2017; Kunkelova *et al.* 2018) and the terrigenous inputs are not so significant (Aubert and Droxler 1992; Purdy and Bertram 1993; Lüdmann *et al.* 2013), especially the fluvial derived material delivered by currents from the Arabian Sea and the Bay of Bengal (Kolla and Rao 1990). We used the Ti/Al elemental ratios to understand terrigenous inputs during the 20 Ma time period. Al and Ti are considered extremely resistant to weathering and are generally used to estimate the abundance of terrigenous materials in sedimentary environments (Murray and Leinen 1996). The Ti/Al ratios from the sites U1467 and U1468 show large variability from 20 to 12 Ma and a gradual increase beginning from ∼12 Ma to recent, punctuated by a drop in ratios at ∼5 Ma. The increase in Ti/Al beginning at ∼12 Ma can be associated with the strengthening of winds and resulting currents associated with initiation of the SAM (Betzler *et al.* 2016). The 10–5 Ma period corresponds to an intense and stable OMZ as seen in the Mn/Ca ratios, which is a result of increased monsoon strength (Betzler *et al.* 2016, figure 2c). This period, based on magnetic susceptibility data shows higher aeolian inputs due to increased wind strength (Betzler *et al.* 2016).

The core site in modern times is a CO_2 source region with an annual sea–air CO_2 flux of 18.7 µatm, highest of which is during the transition (between northeast and southwest monsoon) month of April (Takahashi *et al.* 2009). The planktonic foraminifera *G. trilobus* shell weights were compared to global pCO_2 record which was reconstructed using the following parameters: 'Fluid inclusions' seawater composition data, 'Palike' CCD reconstruction and G17 boron isotopic composition of seawater (Sosdian *et al.* 2018). The sediment cores used in this reconstruction are mostly from oceanic regions wherein the surface seawater is in equilibrium with atmospheric CO_2 and hence the reconstructed pCO_2 is a data of atmospheric CO_2 variability (figure 2b). This is the first record of planktonic foraminifera shell weight covering the Miocene to Pleistocene. Broadly, the shell weight record from sites U1467 and Site U1468 follows a trend opposite to the atmospheric CO_2 trend. The MCO was a period of global warmth with increased CO_2 concentrations in the atmosphere of ∼600 ppm (Greenop *et al.* 2014) and pH as low as 7.6 (Sosdian *et al.* 2018). The shell weight record during MCO is in general lighter in comparison to the entire 20 Ma record. However, within the MCO there are a couple of shell weight data at ∼16 Ma which are slightly heavier. The MCO had large CO_2 variations of up to 400 ppm (Greenop *et al.* 2014) and the slightly heavier shells from the present study correspond to the CO_2 lows within the MCO (figure 2a). The transition from this warmer climate to the modern icehouse world was marked by the MMCT (15–12.5 Ma) where East Antarctic ice sheet (EAIS) expanded and the climate cooled with an associated decline in CO_2 (Foster *et al.* 2012), primarily due to the sequestration of carbon in Monterey Formation of California (Vincent and Berger 1985) and probably some amount due to the silicate weathering of Himalayas (Raymo 1994). This led to an increase in the oceanic pH to ∼8.1 at ∼12.5 Ma (Sosdian *et al.* 2018). Shell weights show a sharp increase at the beginning of the MMCT and peaking at ∼12.06 Ma probably related to increase in surface water $[CO_3^{2-}]$ as a result of CO_2 decline. The shell weights in general were heavier during the glacial periods from Mi 2 to Mi 6 (Miller *et al.* 1991) when atmospheric CO_2 was lower.

The period from ∼12 to 10.5 Ma shows a steep drop in shell weights with an associated drop in $CaCO_3$% at ∼10.5 Ma. This period between 12 and 10 Ma is documented as an intense carbonate impoverishment period, termed as the 'carbonate crash' by Lyle *et al.* (1995), and seen in all major tropical ocean basins with prolonged episodes of reduced carbonate deposition (Lübbers *et al.* 2019). This implies that global changes in the intensity of chemical weathering and riverine input of calcium and carbonate ions into the ocean reservoir were instrumental in driving the carbonate crash (Lübbers *et al.* 2019). An increase in organic export flux is also documented at the same time due to increase in monsoon intensity (Lübbers *et al.* 2019). SEM images at this interval show a clear dissolution of spines in foraminifera (figure 3a).

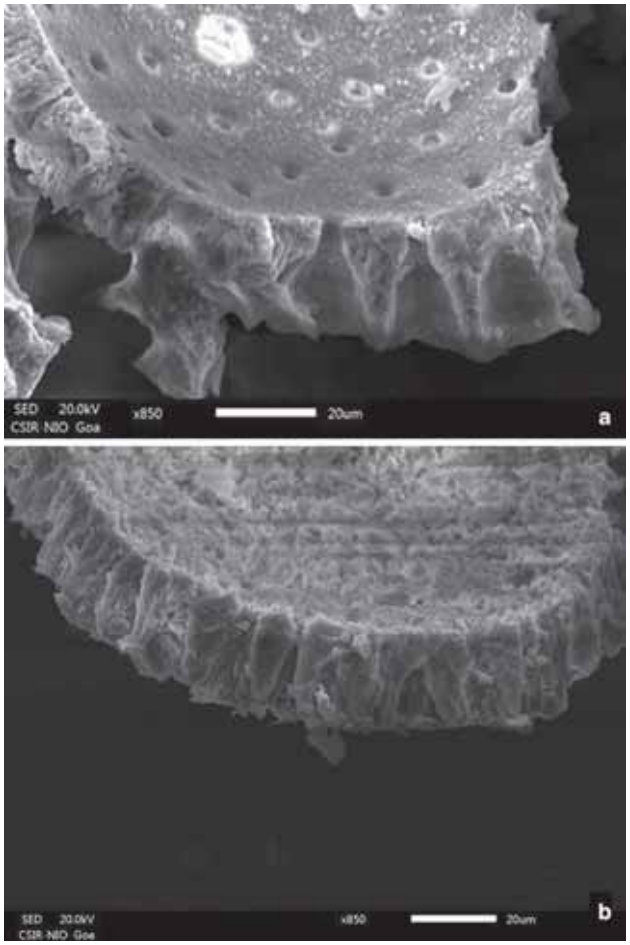

Figure 3. SEM micrographs of *G. trilobus* wall with a magnification of 850× at **(a)** 7.7 Ma, which is from within the intense OMZ period and **(b)** 10.5 Ma, which is the 'carbonate crash' event. Dissolution of spines is seen in both the samples; however, the sample at 10.5 shows relatively more dissolved spines.

Dissolution may take place as the shells pass the sediment–water interface wherein there is an intense organic matter respiration (de Villiers 2005). Betzler *et al.* (2016) have shown the period of ∼12.9 Ma (which is slightly prior to the 12 Ma period where carbonate dissolution begins) to be the switch from sea-level controlled platform growth to the current-dominated sedimentation. We see a large increase in OC% during the 10 Ma event which is close to the high productivity event of 10–8 Ma observed in the Indian Ocean (Gupta *et al.* 2004).

For the period of ∼9 to 3 Ma, surface ocean pH remained between ∼8.0 and 8.1 (Sosdian *et al.* 2018). There is a CO_2 peak at ∼9 Ma which is not seen in any climate records (Sosdian *et al.* 2018). This peak however reflects in our shell weight records showing a shell weight decrease. This period also encompasses the CO_2–climate decoupling period as suggested by Pagani *et al.* (1999). Furthermore, the period from ∼10 to 5 Ma is a period of stable OMZ conditions as seen from Mn/Ca elemental ratios at sites U1466, U1468 and U1471 (Betzler *et al.* 2016, figure 2c). Mn/Ca ratios in general show a drop from 20 Ma up to ∼10 Ma (Betzler *et al.* 2016). After which they remain low up to 5 Ma, indicating that this was the time of intense OMZ in the Maldives Sea. It has been shown that OMZs are associated with high CO_2 which is defined as a carbon maximum zone (CMZ) (Paulmier *et al.* 2011). The present cores being recovered from the OMZ will have a buildup of carbon during this period of intense and stable OMZ. Superimposed on the anti-correlation with CO_2 at specific periods, shell weights during this period from 10 to 5 Ma show large fluctuations and are on an average lighter, probably as a result of calcite dissolution after settling into sediments as a result of build-up of CO_2 in bottom waters. SEM micrograph of *G. trilobus* shell wall at 7.7 Ma shows dissolution of spines but with relatively less intensity in comparison to shells at 10.5 Ma (figure 3b). Furthermore, the OMZ is known to reach its modern strength at about ∼1.0 Ma closely following the enhanced surface water productivity (Tripathi *et al.* 2017) which implies that SAM intensified from ∼1.0 Ma (Derry and France-Lanord 1996; Clift *et al.* 2008). The increased OMZ intensity from ∼1.0 Ma again created conditions favourable for increase in bottom water CO_2 leading to dissolution of shells which reflects in lower shell weights for the past 1 Ma.

Early Pliocene $\delta^{11}B$ based pCO_2 values between 4.6 and 3.6 Ma were above a suggested threshold of 280 ppm below which Northern Hemisphere glaciations are possible (De Conto *et al.* 2008). This was a period of prolonged warmth terminating at ∼2.7 Ma. Atmospheric CO_2 decreased to minimum of 245 ppm at 3.32 Ma after which the Northern Hemisphere glaciations began (Bartoli *et al.* 2011) and subsequently lead to the glacial–interglacial climate variability in the Pleistocene (Lisiecki and Raymo 2005). Shell weights from our core sites remained low from ∼5 to 3 Ma after which they increased in conjunction with the decrease in atmospheric CO_2 and the initiation of NHG, peaking at ∼1 Ma and a sharp decrease thereafter.

Finally, in order to look at a natural analogue of the near future of ocean acidification, we observed shell weights during the MCO, the period of highest atmospheric CO_2 concentrations during the last

20 Ma. Lightest shell weights of ∼15.5 µg occurred at 15.08 Ma when atmospheric CO_2 was ∼500 ppm (figure 2a and b) during the MCO. In comparison, pre-industrial shell weights were ∼17 µg with atmospheric CO_2 concentrations at ∼280 ppm. However, we do not have any record of present day shell weights in this region which would be an interesting comparison to elucidate ocean acidification.

6. Conclusions

The Ti/Al ratios from sites U1467 and U1468, suggest an increase in terrigenous inputs to the Maldives Sea beginning from ∼12 Ma which is in line with strengthening of winds associated with initiation of SAM. Shell weights of *G. trilobus* from these sites negatively co-vary with global atmospheric CO_2 throughout most of the period from Miocene to Pleistocene which suggests that the Maldives Sea behaved similar to other tropical regions of the world throughout the 20 Ma period in terms of its carbonate chemistry. It also shows that the primary control on shell calcification is surface water carbonate ion concentration. The carbonate impoverishment as seen in all major tropical ocean basins between 12 and 10 Ma is documented in the present study by lighter foraminifera shells and visual dissolution of spines. During periods of intense OMZ, shell dissolution due to corrosive bottom waters appears to obscure the understanding of surface water carbonate ion concentrations.

Acknowledgements

We thank IODP for the core samples and IODP-India for funding this study. This is NIO contribution No. 6476. This is IODP-India grant number NCAOR/IODP/2017/8. We thank Mascarenhas-Pereira M B L for the ICP facility.

References

Aubert O and Droxler A 1992 General Cenozoic evolution of the Maldives carbonate system (equatorial Indian Ocean); *Bull. Cent. Rech. Explor.-Prod. Elf-Aquitaine* **16** 113–136.

Backman J, Raffi I, Rio D, Fornaciari E and Pälike H 2012 Biozonation and biochronology of Miocene through Pleistocene calcareous nannofossils from low and middle latitudes; *Newslett. Stratigr.* **45(3)** 221–244, https://doi.org/10.1127/0078-0421/2012/0022.

Barker S and Elderfield H 2002 Foraminiferal calcification response to glacial–interglacial changes in atmospheric CO_2; *Science* **297** 833–836, http://doi.org/10.1126/science.1072815.

Bartoli G, Hönisch B and Zeebe R E 2011 Atmospheric CO_2 decline during the Pliocene intensification of Northern Hemisphere glaciations; *Paleoceanogr.* **26** PA4213, https://doi.org/10.1029/2010PA002055.

Beer C J, Schiebel R and Wilson P A 2010 Testing planktic foraminiferal shell weight as a surface water $[CO_3^{2-}]$ proxy using plankton net samples; *Geology* **38(2)** 103–106, https://doi.org/10.1130/G30150.1.

Betzler C, Eberli G P, Kroon D, Wright J D, Swart P K, Nath B N, Alvarez-Zarikian C A, Alonso-García M, Bialik O M, Blättler C L, Guo J A, Haffen S, Horozal S, Inoue M, Jovane L, Lanci L, Laya J C, Hui Mee A L, Lüdmann T, Nakakuni M, Niino K, Petruny L M, Pratiwi S D, Reijmer J J G, Reolid J, Slagle A L, Sloss C R, Su Xiang, Yao Z and Young J R 2016 The abrupt onset of the modern South Asian Monsoon winds; *Sci. Rep.* **6** 29838, http://doi.org/10.1038/srep29838.

Betzler C, Eberli G P, Alvarez Zarikian C A, Alonso-García M, Bialik O M, Blättler C L, Guo J A, Haffen S, Horozal S, Inoue M, Jovane L, Kroon D, Lanci L, Laya J C, Ling Hui Mee A, Lüdmann T, Nakakuni M, Nath B N, Niino K, Petruny L M, Pratiwi S D, Reijmer J J G, Reolid J, Slagle A L, Sloss C R, Su X, Swart P K, Wright J D, Yao Z and Young J R 2017 Expedition 359 summary; In: *The Expedition 359 Scientists, Maldives Monsoon and Sea Level* (eds) Betzler C, Eberli G P and Alvarez Zarikian C A, *Proceedings of the International Ocean Discovery Program* **359**, https://doi.org/10.14379/iodp.proc.359.101.2017.

Betzler C, Eberli G P, Lüdmann T, Reolid J, Kroon D, Reijmer J J G, Swart P K, Wright J, Young J R, Alvarez-Zarikian C A, Alonso-García M, Bialik O M, Blättler C L, Guo J A, Haffen S, Horozal S, Inoue M, Jovane L, Lanci L, Laya J C, Hui Mee A L, Nakakuni M, Nath B N, Niino K, Petruny L M, Pratiwi S D, Slagle A L, Sloss C R, Su Xiang and Yao Z 2018 Refinement of Miocene sea level and monsoon events from the sedimentary archive of the Maldives (Indian Ocean); *Progr. Earth Planet. Sci.* **5** 5, http://doi.org/10.1186/s40645-018-0165-x.

Bialik O M, Frank M, Betzler C, Zammit R and Waldmann N D 2019 Two-step closure of the Miocene Indian Ocean gateway to the Mediterranean; *Sci. Rep.* **9** 8842, https://doi.org/10.1038/s41598-019-45308-7.

Bunzel D, Schmiedl G, Lindhorst S, Mackensen A, Reolid J, Romahn S and Betzler C 2017 A multi-proxy analysis of Late Quaternary ocean and climate variability for the Maldives, Inner Sea; *Clim. Past* **13(12)** 1791–1813, https://doi.org/10.5194/cp-13-1791-2017.

Clift P D, Hodges K V, Heslop D, Hannigan R, Long H V and Calves G 2008 Correlation of Himalayan exhumation rates and Asian monsoon intensity; *Nat. Geosci.* **1** 875–880, http://doi.org/10.1038/ngeo351.

de Villiers S 2004 Occupation of an ecological niche as the fundamental control on the shell-weight of calcifying planktonic foraminifera; *Mar. Biol.* **144(1)** 45–50, https://doi.org/10.1007/s00227-003-1183-8.

de Villiers S 2005 Foraminiferal shell-weight evidence for sedimentary calcite dissolution above the lysocline; *Deep-Sea Res., Part I: Oceanogr. Res. Papers* **52(5)** 671–680, https://doi.org/10.1016/j.dsr.2004.11.014.

De Conto R M, Pollard D, Wilson P A, Pälike H, Lear C H and Pagani M 2008 Thresholds for Cenozoic bipolar glaciation; *Nature* **455** 652–657, http://doi.org/10.1038/nature07337.

Derry L A and France-Lanord C 1996 Neogene Himalayan weathering history and river $^{87}Sr/^{86}Sr$: Impact on the marine Sr record; *Earth Planet. Sci. Lett.* **142** 59–74, https://doi.org/10.1016/0012-821X(96)00091-X.

Flower B P and Kennett J P 1994 The middle Miocene climatic transition: East Antarctic ice sheet development, deep ocean circulation and global carbon cycling; *Palaeogeogr. Palaeoclimatol. Palaeoecol.* **108** 537–555, https://doi.org/10.1016/0031-182(94)90251-8.

Fluteau F, Ramstein G and Besse J 1999 Simulating the evolution of the Asian and African monsoons during the past 30 Myr using an atmospheric general circulation model; *J. Geophys. Res.* **104** 11,995–12,018, https://doi.org/10.1029/1999JD900048.

Foster G L, Lear C H and Rae J W B 2012 The evolution of pCO_2, ice volume and climate during the middle Miocene; *Earth Planet. Sci. Lett.* **341–344** 243–254, https://doi.org/10.1016/j.epsl.2012.06.007.

Goyet G, Metzl N, Millero F J, Eischeid d, Sullivan O' and Poisson A 1998 Temporal variation of the sea surface CO_2/carbonate properties in the Arabian Sea; *Mar. Chem.* **63** 69–79, https://doi.org/10.1016/S0304-4203(98)00051-6.

Greenop R, Foster G L, Wilson P A and Lear C H 2014 Middle Miocene climate instability associated with high-amplitude CO_2 variability; *Paleoceanography* **29** 845–853, https://doi.org/10.1002/2014PA002653.

Gupta A K, Singh R K, Joseph S and Thomas E 2004 Indian Ocean high-productivity event (10–8 Ma): Linked to global cooling or to the initiation of the Indian monsoons?; *Geology* **32** 753–756, https://doi.org/10.1130/G20662.1.

Gupta A K, Yuvaraja A, Prakasam M, Clemens S C and Velu A 2015 Evolution of the South Asian monsoon wind system since the late Middle Miocene; *Palaeogeogr. Palaeoclimatol. Palaeoecol.* **438** 160–167, https://doi.org/10.1016/j.palaeo.2015.08.006.

Holbourn A, Kuhnt W, Schulz M and Erlenkeuser H 2005 Impacts of orbital forcing and atmospheric carbon dioxide on Miocene ice-sheet expansion; *Nature* **438** 483–487, https://doi.org/10.1038/nature04123.

Kroon D, Steens T and Troelstra S R 1991 Onset of monsoonal related upwelling in the western Arabian Sea as revealed by planktonic foraminifers; *Proc. Ocean Drill. Prog. Sci. Res.* **117** 257–263, http://doi.org/10.2973/odp.proc.sr.117.126.1991.

Kunkelova T, Jung S J A, de Leau E S, Odling N, Thomas A L, Betzler C, Eberli G P, Alvarez-Zarikian C A, Alonso-García M, Bialik O M, Blättler C L, Guo J A, Haffen S, Horozal S and Mee A L H 2018 A two million year record of low-latitude aridity linked to continental weathering from the Maldives; *Prog. Earth Planet. Sci.* **5** 86, https://doi.org/10.1186/s40645-018-0238-x.

Kolla V and Rao N M 1990 Sedimentary sources in the surface and near-surface sediments of the Bay of Bengal; *Geo-Mar. Lett.* **10(3)** 129–135, https://doi.org/10.1007/978-1-4020-6646-7_5.

Lindhorst S, Betzler C and Kroon D 2019 Wind variability over the northern Indian Ocean during the past 4 million years – Insights from coarse aeolian dust (IODP exp. 359, site U1467, Maldives); *Palaeogeogr. Palaeoclimatol. Palaeoecol.* **536** 109371, https://doi.org/10.1016/j.palaeo.2019.109371.

Lisiecki L E and Raymo M E 2005 A Pliocene–Pleistocene stack of 57 globally distributed benthic $\delta^{18}O$ records; *Paleoceanogr.* **20** PA1003, http://doi.org/10.1029/2004PA001071.

Lyle M, Dadey K A and Farrell J W 1995 The late Miocene (11–8 Ma) Eastern Pacific carbonate crash: Evidence for reorganization of deep-water circulation by the closure of the Panama Gateway; In: *Proc. Ocean Drill. Prog. Sci. Res.* (eds) Pisias N G, Mayer L A, Janecek T R, Palmer-Julson A and van Andel T H, College Station TX (Ocean Drilling Program) **138** 821–838, http://doi.org/10.2973/odp.proc.sr.138.157.1995.

Lübbers J, Kuhnt W, Holbourn A E, Bolton C T, Gray E, Usui Y, Kochhann K G D, Beil S and Andersen N 2019 The Middle to Late Miocene 'Carbonate Crash' in the Equatorial Indian Ocean; *Paleoceanogr. Paleoclimatol.* **34** 813–832, https://doi.org/10.1029/2018PA003482.

Lüdmann T, Kalvelage C, Betzler C, Fürstenau J and Hübscher C 2013 The Maldives, a giant isolated carbonate platform dominated by bottom currents; *Mar. Petrol. Geol.* **43** 326–340, http://dx.doi.org/10.1016/j.marpetgeo.2013.01.004.

Martini E 1971 Standard Tertiary and Quaternary calcareous nannoplankton zonation; In: *Proc. II Planktonic Conference, Roma 1970, Roma, Tecnoscienza* **2** 739–785.

Maslin M A, Li X S, Loutre M F and Berger A 1998 The contributon of orbital forcing to the progressive intensification of Northern Hemisphere glaciation; *Quat. Sci. Rev.* **17** 411–426, https://doi.org/10.1016/S0277-3791(97)00047-4.

Miller K G, Wright J D and Fairbanks R G 1991 Unlocking the Ice House: Oligocene–Miocene oxygen isotopes, eustacy and margin erosion; *J. Geophys. Res.* **96** 6829–6848, https://doi.org/10.1029/90JB02015.

Miller K G, Kominz M A, Browning J V, Wright J D, Mountain G S, Katz M E, Sugarman P J, Cramer B S N, Christie-Blick N and Pekar S F 2005 The phanerozoic record of global sea-level change; *Science* **310** 1293–1298, http://doi.org/10.1126/science.1116412.

Murray R W and Leinen M 1996 Scavenged excess aluminum and its relationship to bulk titanium in biogenic sediment from the central equatorial Pacific Ocean; *Geochim. Cosmochim. Acta* **60(20)** 3869–3878.

Naik S S, Naidu P D, Govil P and Godad S 2010 Relationship between weights of planktonic foraminifer shell and surface water $CO_3^{=}$ concentration during the Holocene and Last Glacial period; *Mar. Geol.* **275** 278–282, https://doi.org/10.1016/j.margeo.2010.05.004.

Naik S S, Godad S P, Naidu P D and Ramaswamy V 2013 A comparision of *Globigerinoides ruber* calcification between upwelling and non-upwelling regions in the Arabian Sea; *J. Earth Syst. Sci.* **122** 1153–1159, http://doi.org/10.1007/s12040-013-0330-y.

Nigam R and Heriques P J 1992 Planktonic percentage of foraminiferal fauna in surface sediments of the Arabian Sea (Indian Ocean) and a regional model for paleodepth

determination; *Palaeogeogr. Palaeoclimatol. Palaeoecol.* **91(1–2)** 89–98.

Pagani M, Arthur M A and Freeman K H 1999 Miocene evolution of atmospheric carbon dioxide; *Paleoceanogr.* **14** 273–292, http://doi.org/10.1029/1999PA900006.

Paulmier A, Ruiz-Pino D and Garçon V 2011 CO_2 maximum in the oxygen minimum zone (OMZ); *Biogeosci.* **8** 239–252, http://doi.org/10.5194/bg-8-239-2011.

Purdy E G and Bertram G T 1993 Carbonate concepts from the Maldives, Indian Ocean; *AAPG Stud. Geology* **34** 7–55, https://doi.org/10.1306/St34568.

Raffi I, Backman J, Fornaciari E, Pälike H, Rio D, Lourens L and Hilgen F 2006 A review of calcareous nannofossil astrobiochronology encompassing the past 25 million years; *Quat. Sci. Rev.* **25** 3113–3137; https://doi.org/10.1016/j.quascirev.2006.07.007.

Ramstein G, Fluteau F, Besse J and Joussaume S 1997 Effect of orogeny, plate motion and land–sea distribution on Eurasian climate change over the past 30 million years; *Nature* **386** 788–795, https://doi.org/10.1038/386788a0.

Raymo M E 1994 The Himalayas, organic carbon burial, and climate in the Miocene; *Paleoceanogr.* **9** 399–404, https://doi.org/10.1029/94PA00289.

Sarma V V S S 2003 Monthly variablity in surface pCO_2 and net air-sea CO_2 flux in the Arabian Sea; *J. Geophys. Res.* **108**, https://doi.org/10.1029/2001JC001062.

Sarma V V S S, Lenton A, Law R M, Metzl N, Patra P K, Doney S, Lima L D, Dlugokencky E, Ramonet M and Valsala V 2013 Sea–air CO_2 fluxes in the Indian Ocean between 1990 and 2009; *Biogeosciences* **10** 7035–7052, https://doi.org/10.5194/bg-10-7035-2013.

Schulte S, Rostek F, Bard E, Rullkötter J and Marchal O 1999 Variations of oxygen-minimum and primary productivity recorded in sediments of the Arabian Sea; *Earth Planet. Sci. Lett.* **173** 205–221, https://doi.org/10.1016/S0012-821X(99)00232-0.

Sosdian S M, Greenop R, Hain M P, Foster G L, Pearson P N and Lear C H 2018 Constraining the evolution of Neogene ocean carbonate chemistry using the boron isotope pH proxy; *Earth Planet. Sci. Lett.* **498** 362–376, https://doi.org/10.1016/j.epsl.2018.06.017.

Takahashi T, Sutherland S C, Wanninkhof R, Sweeney C, Feely R A, Chipman D W, Hales B, Friederich G, Chavez F, Sabine C, Watson A, Bakker D C E, Schuster U, Metzl N, Yoshikawa-Inoue H, Ishii M, Midorikawa T, Nojiri Y, Körtzinger A, Steinhoff T, Hoppema M, Olafsson J, Arnarson T S, Tilbrook B, Johannessen T, Olsen A, Bellerby R, Wong C S, Delille B, Bates N R and de Baar H J W 2009 Climatological mean and decadal change in surface ocean pCO_2, and net sea–air CO_2 flux over the global oceans; *Deep-Sea Res. II* **56** 554–577, https://doi.org/10.1016/j.dsr2.2008.12.009.

Tomczak M and Godfrey J S 2003 *Regional oceanography: An introduction*; Daya Publishing House, New Delhi, India, 401p, http://doi.org/10.1016/B978-0-08-041021-0.50010-2.

Tripathi S, Tiwari M, Lee J, Khim B-K and IODP Expedition 355 Scientists 2017 First evidence of denitrification vis-à-vis monsoon in the Arabian Sea since Late Miocene; *Sci. Rep.* **7** 43056, http://doi.org/10.1038/srep43056.

van Hinsbergen D J J, de Groot L V, van Schaik S J, Spakman W, Bijl P K, Sluijs A, Langereis C G and Brinkhuis H 2015 A Paleolatitude calculator for paleoclimate studies; *PLoS ONE* **10** 1–21, https://doi.org/10.1371/journal.pone.0126946.

Vincent E and Berger W H 1985 Carbon dioxide and polar cooling in the Miocene: The Monterey hypothesis; In: *The Carbon Cycle and Atmospheric CO_2: Natural Variations Archean to Present* (eds) Sundquist E T and Broecker W S, American Geophysical Union, Washington DC, pp. 455–468, https://doi.org/10.1029/GM032p0455.

Zhisheng A, Kutzbach J E, Prell W L and Porter S C 2001 Evolution of Asian monsoons and phased uplift of the Himalaya–Tibetan plateau since Late Miocene times; *Nature* **411** 62–66, http://doi.org/10.1038/35075035.

Corresponding editor: N V Chalapathi Rao